Comparisons of Line-of-Sight Water Vapor Observations Using the Global Positioning System and a Pointing Microwave Radiometer

JOHN BRAUN AND CHRISTIAN ROCKEN

GPS Research Group, University Corporation for Atmospheric Research, Boulder, Colorado

JAMES LILJEGREN

Environmental Research Division, Argonne National Laboratory, Argonne, Illinois

(Manuscript received 28 May 2002, in final form 15 October 2002)

ABSTRACT

Line-of-sight measurements of integrated water vapor from a global positioning system (GPS) receiver and a microwave radiometer are compared. These two instruments were collocated at the central facility of the Department of Energy's Atmospheric Radiation Measurement Program's Southern Great Plains region, near Lamont, Oklahoma. The comparison was made using 47 days of observations in May and June of 2000. Weather conditions during this time period were variable with total integrated water vapor ranging from less than 10 to more than 50 mm. To minimize errors in the microwave radiometer observations, observations were compared during conditions when the liquid water measured by the radiometer was less than 0.1 mm. The linear correlation of the observations between the two instruments is 0.99 with a root-mean-square difference of the GPS water vapor to a linear fit of the microwave radiometer of 1.3 mm. The results from these comparisons are used to evaluate the ability of networks of GPS receivers to measure instantaneous line-of-sight integrals of water vapor. A discussion and analysis is provided regarding the additional information of the water vapor field contained in these observations compared to time- and space-averaged zenith and gradient measurements.

1. Introduction

The development of new techniques to measure water vapor in the earth's atmosphere has been identified as a key research area in atmospheric sciences (Dabberdt and Schlatter 1996; Emanuel et al. 1995). The ability to measure the integrated amount of water vapor along the line-of-site path between a ground-based global positioning system (GPS) receiver and a transmitting GPS satellite holds the potential to provide detailed and precise observations for the characterization and monitoring of atmospheric water vapor. This line-of-sight integral is commonly called slant water (SW; Ware et al. 1997; Braun et al. 2001). One proposed application of SW is to deploy a dense network of GPS stations in a region, measure SW from each of the stations to all visible satellites, and combine them to retrieve the three dimensional water vapor field above the network (MacDonald et al. 2002).

An SW observation can be represented as a sum of two components. The first component is the isotropic portion, and is essentially the vertically integrated precipitable water vapor (PW) that is now routinely estimated using GPS (Bevis et al. 1992; Rocken et al. 1993; Wolfe and Gutman 2000). Precipitable water can be considered the average of all SW observations to all GPS satellites observed from a site and over a period of time scaled to zenith. Typical PW estimation assumes that the water vapor field is horizontally homogeneous and temporally unchanging during the time period for which the individual observations are averaged. This assumption is always incorrect at some level and the second component of SW describes the deviation of the water vapor field from the isotropic PW field. This term can be determined using several strategies. One way is to estimate time varying gradient parameters that model the spatial variability of water vapor (Bar-Sever et al. 1998). Like a PW measurement this technique combines observations to reduce measurement noise but depending on the gradient model, sacrifices spatial resolution. A second method is to directly compute the unmodeled delay along the line-of-sight path between a GPS receiver and transmitting satellite. This technique does not benefit from any averaging, but it can retrieve features that are not adequately described by a time varying atmospheric gradient. A combination of the two techniques may also be used. Slant water can be represented as a sum of the isotropic and nonisotropic terms:

Corresponding author address: John Braun, GPS Science and Technology Group, University Corporation for Atmospheric Research, PO Box 3000, Boulder, CO 80307.
E-mail: braunj@ucar.edu

$$\mathrm{SW}_i^j(\theta) = m(\theta_i^j)\mathrm{PW}_i + S_i^j,$$

where SW_i^j is the slant water vapor along the path between station i and satellite j, PW_i is the precipitable water vapor at station i, $m(\theta_i^j)$ is the mapping function that relates the zenith PW value to the elevation angle (θ_i^j) of the satellite j in relation to the station i (Niell 1996; Rocken et al. 2001), and S_i^j is the nonisotropic component of water vapor for station i and satellite j. The difficulty in measuring SW as compared to PW is that the noise of SW is not reduced by averaging over time and multiple satellites. Without this averaging, error sources such as receiver and transmitter clock errors, ground reflected multipath, and antenna phase center mismodeling can cause errors in SW that may be larger than the nonisotropic term (S_i^j). This is true whether S_i^j is determined using gradient parameters or the unmodeled line-of-sight delay. In the instances when measurement noise dominates over the magnitude of S_i^j, SW offers no more information than PW scaled to the appropriate elevation angle of the satellite.

In a previous study by Braun et al. (2001), the nonisotropic portion of SW was computed at a GPS station and a collocated water vapor microwave radiometer (WVR) and then compared against each other. This experiment was limited to three days of data taken along the Colorado Front Range where the atmosphere contained only a modest amount of water vapor. The average amount of PW during this comparison was just 18 mm and the largest magnitude of the S_i^j component of SW was less than 10 mm. While the results from this experiment were encouraging, the technique of measuring SW using GPS needed to be verified with a larger data set and under a wider range of conditions. In the study presented here, 47 days of data collected at the Department of Energy's Atmospheric Radiation Measurement (ARM) Program's Central Facility near Lamont, Oklahoma, are used to construct a robust comparison of SW.

2. Experiment description

The data from the GPS station at the ARM central facility were included in the analysis of a continental size network to determine the absolute SW. The entire network contained 33 stations; 27 of them were part of the National Oceanic and Atmospheric Administration (NOAA) Forecast Systems Laboratory GPS network (Gutman and Holub 2000). Five of the stations were International GPS Service (IGS) sites that were included to properly tie the network into the International Terrestrial Reference Frame (Altamimi 2001). Final satellite orbits and earth orientation information from the IGS were used (Springer 2001). All data were analyzed with the Bernese 4.2 software (Hugentobler et al. 2001). The carrier phase observations were analyzed on the double difference level to remove satellite and receiver clock errors. A minimum elevation mask of 10° and a sampling rate of 30 were used in the data analysis. Precipitable water estimates were computed using a combined 30 min of observations. Surface pressure measurements and the Saastamoinen model were used to remove the dry delay. The wet Niell mapping function was used to estimate the wet delay (Niell 1996). The scaling factor to relate wet delay to integrated water vapor, commonly known as the Π factor (Bevis et al. 1994), was computed using a surface temperature measurement (T_s, in kelvins) which was converted into a mean atmospheric temperature using $T_m = 0.7013\,T_s + 75.593$. This equation for T_m was derived from an analysis of radiosonde observations within the Southern Great Plains.

After estimation of PW and assuming the station coordinates and orbit errors were negligible the unmodeled part of the data, or residuals, was due to atmospheric variability, antenna phase center variation, and ground reflected multipath. These double-difference residual delays were transformed into line-of-sight delays using the technique described by Alber et al. (2000). The large number of stations used in the analysis, and their distribution throughout the United States improved the quality of the ''zero-mean'' assumptions required for this transformation. Any errors due to these assumptions (if the mean was not zero) were distributed evenly over all the stations in the network. In addition to the errors caused by the double difference to zero difference conversion, the zero difference residuals contained the nonisotropic delay, antenna phase center variations, and ground-reflected multipath for each station. The ground reflected multipath and antenna phase center mismodeling was minimized through the use of site-specific multipath maps (Braun et al. 2001). Each map was a composite of the previous 20 days of line-of-sight residuals updated daily by incorporating the most recently processed day of data into the map. This daily update, and a weighting scheme that weighted newer data higher than older data, helped the map adapt to any temporal changes that may have occurred at a station (i.e., due to rain and snow). At elevation angles less than 15°, the corrections were as large as 5 mm in SW. For elevation angles above 15°, the corrections were typically less than 2 mm. The daily variation of the multipath map was small. After applying these map corrections, the residuals represented the delay due to the nonisotropic component of water vapor in the direction of the satellite. This delay was converted into its equivalent amount of nonisotropic water vapor (S_i^j) using the same Π factor used to relate wet delay to PW. These were added to the PW measurements to fully reconstruct the SW measurement. GPS receivers are multichannel instruments. They simultaneously track all satellites which are visible in the sky and provide instantaneous measurements (in this experiment in 30-s intervals) to each satellite.

A Radiometrics WVR-1100 microwave water vapor radiometer with azimuth and elevation pointing capa-

bility was positioned within 20 m of the GPS station at the ARM central facility. This instrument was operated in a mode that performed a tip curve for calibration (Liljegren 2000), and then sequentially pointed in the direction of all GPS satellites higher than 10° above the horizon. The algorithm used to point the radiometer towards a particular GPS satellite was optimized to cycle through all satellites in the minimum amount of time. Each cycle of calibration and observations would take between 2 and 5 min depending on the number and orientation of all satellites. The beamwidth for the radiometer is about 6° for the water vapor channel (23.8 GHz) and 4.5° for the liquid water channel (31.4 GHz). The elevation mask of 10° was chosen to minimize any brightness temperature errors due to ground pickup. The continuous tip curve calibration limited the largest possible beam pointing errors to one motor step, 0.45° per step (Liljegren 2000).

The WVR observations were screened to remove sections of data when the instrument measured more than 0.1 mm of liquid water in the atmosphere, or when liquid water was detected on the Teflon window using an integrated circuit mounted on top of the radiometer. This editing was done to remove periods when the relatively large brightness temperature of condensed water might have contaminated the WVR observation. There were more than 128 000 WVR SW observations; approximately 15% of these were rejected due to the liquid water screening. The WVR measured SW directly. To compare the WVR nonisotropic SW to GPS, the PW had to be computed and removed from each measurement of SW. To be consistent with the GPS, all measurements of SW from the WVR were scaled to zenith and combined into 30-min time windows. This average was taken to be the PW as measured by the WVR. The half hour PW estimates were then linearly interpolated to each observation time and subtracted from the SW value to determine S_i^j.

3. Results

Figure 1 shows a scatterplot of both SW and PW from GPS against SW from the WVR. The half-hour estimates of GPS PW were linearly interpolated to match the time tags of the more frequently measured WVR SW. GPS SW, which were available every 30 s, were matched in time to the nearest WVR measurement which were available every 2–5 min. Both the PW and SW have been scaled to their equivalent zenith value so that all the observations can be compared without regard to the satellite elevation angle. There are more than 107 000 points of PW and SW in Fig. 1. The magnitude of zenith scaled SW ranges from less than 10 mm to more than 50 mm, with a mean of 31 mm. Figure 1 is a composite of the entire 47 days of data, including periods of heterogeneous and more variable atmospheric conditions. Within this broad range of atmospheric conditions, the GPS SW agrees with the WVR SW better than the linearly interpolated GPS PW. This can be numerically quantified as the root-mean square (rms) of the GPS SW (or PW) to a linear fit of the WVR SW. The rms of the linear fit of the GPS PW is 1.4 mm and the GPS SW is 1.3 mm. This difference is not large, but it is consistent for the entire dataset and implies that SW is a better representation of the actual atmospheric water vapor distribution than PW. The linear correlation coefficient of both the PW and SW from GPS to the WVR SW is 0.99. This statistically demonstrates the good agreement between the two instruments. The measurement of SW is only an improvement to PW when the S_i^j component of SW is larger than the noise associated with an individual measurement. To identify time periods with relatively large S_i^j the rms of S_i^j for all WVR measurements was determined to be 0.7 mm. If only the WVR measurements with an S_i^j component of SW greater than 0.7 mm are compared against GPS, the rms of the linear fit becomes 1.9 mm for the GPS PW and 1.7 mm for the GPS SW.

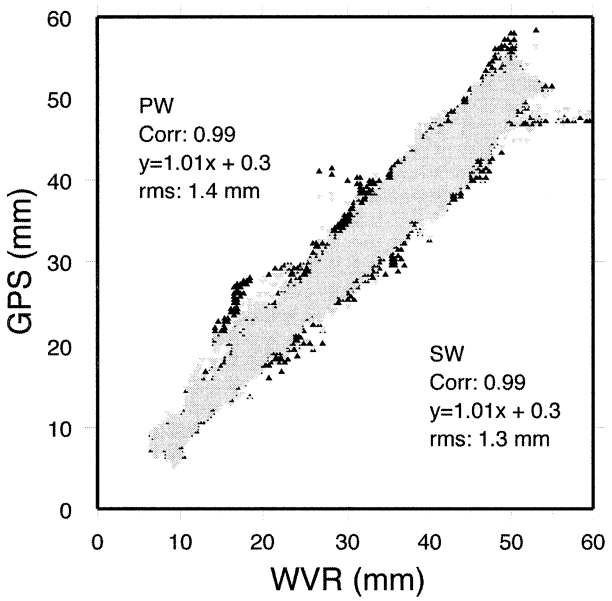

FIG. 1. Scatterplot of GPS PW (black triangles) and GPS SW (gray inverted triangles) as a function of the WVR SW measurement. The GPS and WVR SW have been scaled to their equivalent zenith values so they can be directly compared to the GPS PW. The statistics of the linear regression of the GPS observations to the WVR observations is also shown.

Figure 1 shows a composite of the entire dataset. Individual satellite traces of S_i^j and SW are plotted in Figs. 2 and 3. The top panels in these figures contain S_i^j as measured by the GPS and WVR. In these panels the two instruments were pointing to a single satellite, therefore S_i^j can be compared without scaling to the equivalent zenith value. The agreement of S_i^j as measured by the GPS and WVR demonstrates the ability of the two instruments to resolve water vapor features that are either wetter (positive values of S_i^j) or drier (negative S_i^j) than the rest of the atmosphere at the site. Satellite

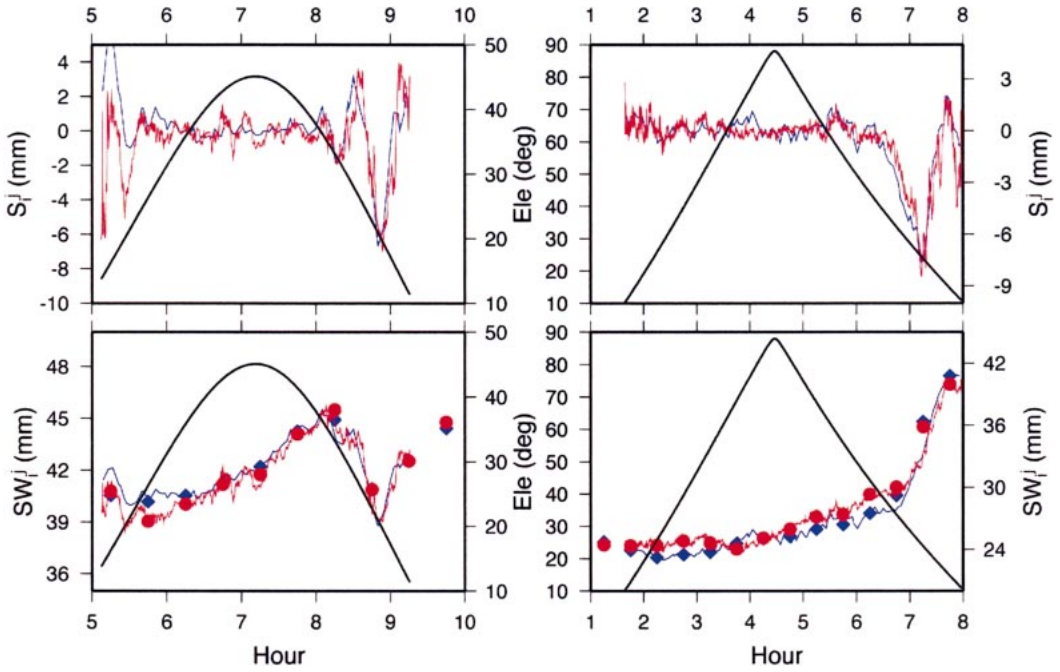

FIG. 2. Time series of GPS and WVR slant water vapor observations in the direction of an individual satellite. The top panel contains the nonisotropic component of SW (S_i^j), GPS in red and WVR in blue. The bottom panel contains the half hour PW measurements (GPS are red dots, WVR are blue diamonds), and the total SW observation. The total SW observation is normalized to the equivalent zenith value so that PW and SW can be plotted on the same scale. Satellite elevation angle is plotted in all panels as the black line.

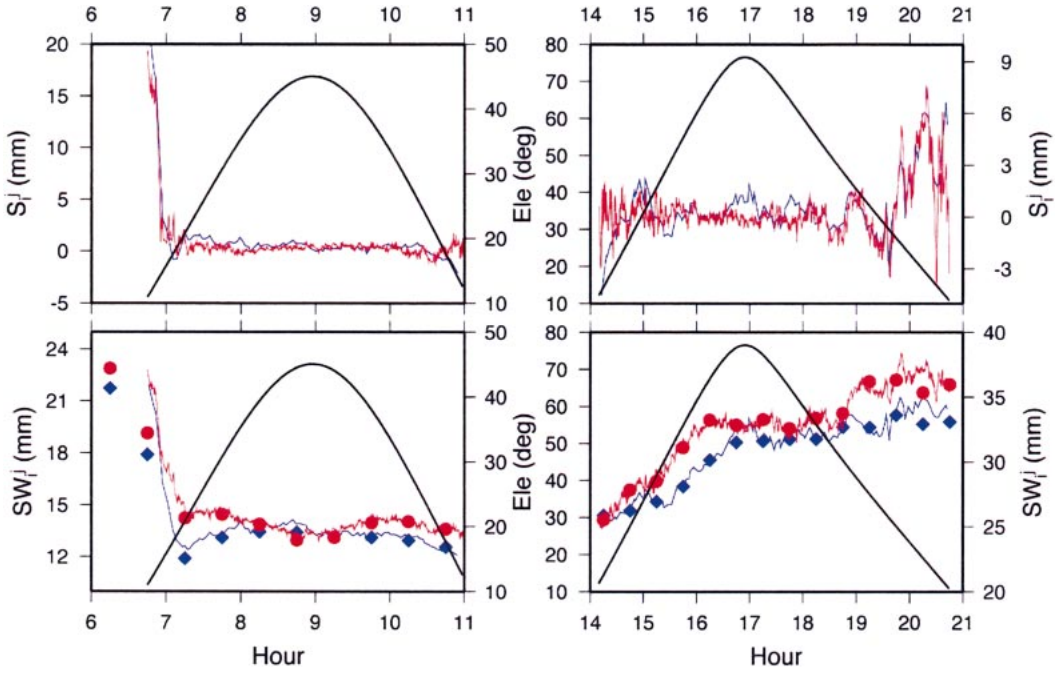

FIG. 3. Same as Fig. 2, but for two different satellite traces.

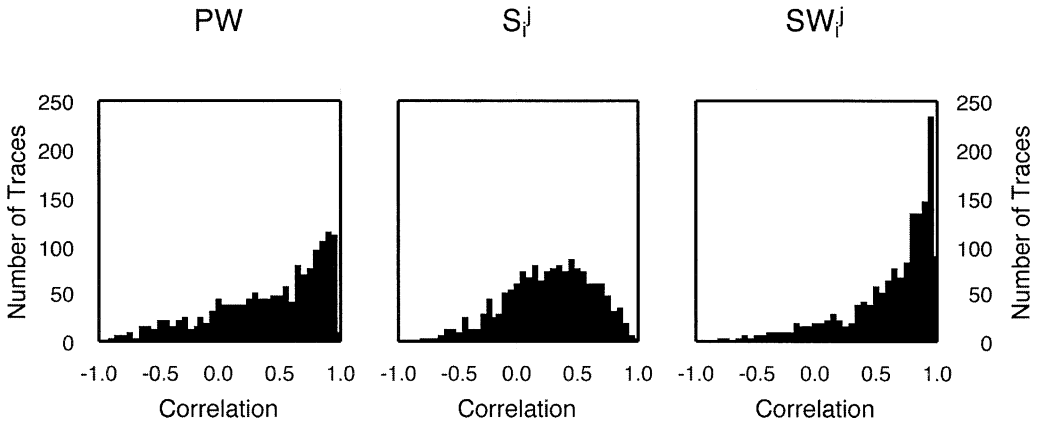

FIG. 4. Histograms of linear correlation coefficients for individual satellite traces. (left) The linear correlation of the GPS PW with respect to WVR SW, (middle) the linear correlation of S_i^j from GPS to the WVR S_i, and (right) the linear correlation of the GPS SW to the WVR SW.

elevation angles are also plotted in Figs. 2 and 3 to indicate the longer paths through the planetary boundary layer. These longer integrals correspond to larger magnitudes of S_i^j. During periods of severe atmospheric heterogeneity, the magnitude of S_i^j was observed to be as large as 20 mm. The bottom panels in Figs. 2 and 3 show total SW. In these panels SW has been scaled to zenith so that PW can also be included for comparison. Figure 2 shows instances where there is good agreement between both S_i^j and SW. Figure 3 shows examples where there is good agreement of S_i^j, but SW is different by up to 5 mm. The disagreement in SW is due to some type of systematic difference between the two instruments. With the continuous calibration of the WVR (Liljegren 2000), it is doubtful that this systematic error is caused by the WVR being misaligned (a pointing error of 0.225° would contribute only a 2.2% error). The reason for these systematic differences is uncertain, but they must be resolved if a network of GPS and WVR instruments is to be deployed together. A simulation of SW using a 3% refractivity variation located 1 km vertically and 2 km horizontally from a GPS station was shown in Ware et al. (1997). This feature induced a 3-mm increase in SW when compared to the isotropic background refractivity. The large variations shown in Figs. 2 and 3 are clearly similar in structure to this simulation, but they contain a much larger signal.

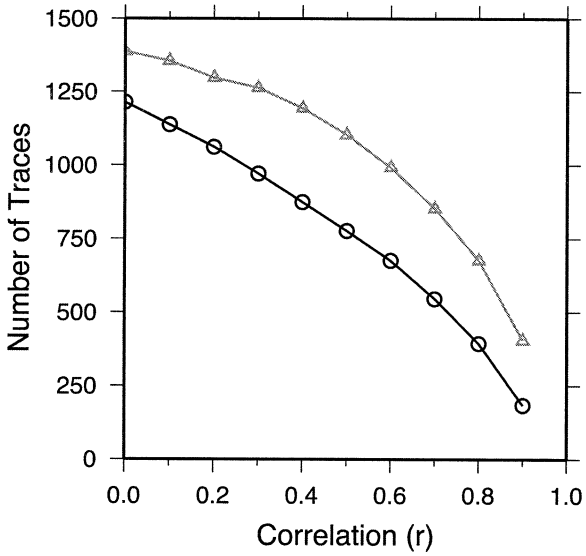

FIG. 5. Number of satellite tracks with linear correlation coefficient greater than r for GPS PW (black) and SW (gray) as compared to the WVR SW. There were 1527 total satellite tracks considered.

To further illustrate the benefit of SW as compared to PW, the correlation coefficients of the following datasets were calculated. First, the linear correlation coefficient (r) comparing GPS PW and WVR SW was computed for each of the 1527 individual satellite traces. Second, the linear correlation of GPS and WVR S_i^j was computed for each individual satellite trace. Finally, the linear correlation of SW measured with GPS and WVR instruments for each trace was computed. These results are summarized in Figs. 4 and 5. In these comparisons it is assumed that the WVR SW is the true representation of the atmosphere. Therefore the comparisons of GPS PW and SW to the WVR SW indicate how well each measurement represents the actual atmosphere. The histogram of S_i^j in Fig. 4 shows that almost all of the satellite tracks have a correlation coefficient greater than 0. This implies that the GPS S_i^j term almost never adds more noise to the GPS SW when compared to PW. Figure 5 shows the number of satellite tracks whose linear correlation coefficient is greater than the specified value of the abscissa. There are more than twice as many SW tracks (404) than PW tracks (184) with $r > 0.9$. When the histograms of the GPS PW and SW are compared against each other, it is clear that the SW satellite traces have a higher correlation to the WVR SW. This improved agreement between the GPS and radiometric measurements of SW can be attributed to the fact that

the GPS SW contains more of the water vapor structure contained by the WVR.

4. Discussion of results

The SW values presented in this paper span a wide range of conditions. The time periods with small amounts of SW, zenith scaled to about 10 mm, are typical for a very dry midlatitude atmosphere. The wettest time periods, with a zenith scaled SW of more than 50 mm, are common in a tropical atmosphere. This broad range was captured in a dataset that contained more than 107 000 observations in 1537 different satellite tracks over 47 days. These characteristics indicate that this analysis is a much more robust comparison than the dataset reported in the Braun et al. (2001) paper.

The method used in this study to determine SW with a GPS receiver relates the unmodeled line-of-sight delay to nonisotropic SW. There are other reasonable techniques to measure S_i^j. For instance, it would be feasible to implement a gradient estimation scheme that uses higher-order terms to detect smaller-scale features. These higher-order gradient terms will always have less spatial resolution than an individual line-of-sight technique. The benefit is that a gradient estimation strategy might contain less noise because it would utilize multiple observations to determine the coefficients of the model. This leads to the fundamental trade off: spatial resolution will be sacrificed to minimize errors associated with a single measurement of SW. Atmospheric boundary layer processes like horizontal convective rolls, moisture transport via low-level jets, and other convective initiation processes will benefit from spatially detailed observations. This implies that a line-of-sight determination of S_i^j might be preferred over gradient strategies for the detection of some important atmospheric features. However, a double difference line-of-sight measurement might be the most precise observation and may be the measurement that is best suited for incorporation into atmospheric models. A double-difference measurement would not be subject to any of the errors associated with satellite or receiver clocks and would not have to rely on the zero mean assumptions which have been used in this analysis and described in Alber et al. (2000). We have chosen to focus on individual station and satellite line-of-sight results because they are simpler to validate and compare to measurements collected with a WVR.

If the entire dataset is considered, the rms of linear fit of the GPS PW was only slightly worse than the rms of the linear fit of SW. When the WVR observations with S_i^j magnitudes greater than one standard deviation of the rms of all S_i^j were considered the difference between the rms of the PW and SW is larger (1.9–1.7 mm). The agreement at two standard deviations is larger still (2.7–2.3 mm). A more qualitative view is shown in the linear correlation coefficients r for each satellite track in Fig. 4. The improvement in r for the individual satellite tracks is clearly evident when the histogram of GPS PW is compared to the histogram of GPS SW. The broad width of the S_i^j histogram is attributed to the frequent time periods when the atmosphere was essentially homogeneous and the portion of SW attributed to S_i^j was small. However most of the S_i^j correlation coefficients are greater than 0, indicating that the S_i^j term rarely degrades a SW measurement.

The WVR was chosen as the reference instrument to measure SW because of the direct nature in which the instrument measures SW, and their wider acceptance in the scientific community. However, liquid water in the atmosphere or condensed water on the viewing window of the radiometer can cause significant errors in the WVR measurements. In this experiment approximately 15% of the WVR data were excluded due to liquid water contamination. GPS is essentially insensitive to liquid water (Solheim et al. 1999). This implies that GPS can be used to determine SW in all weather conditions. An inspection of all the GPS SW measurements revealed significant water vapor variations when the WVR measured liquid water greater than 0.1 mm. Clearly these were times when there was liquid in the atmosphere and/or there was water on the WVR viewing window. During these times, it can be assumed that the GPS was working well and that SW from GPS was accurate. Given that GPS is an all-weather sensor, the SW in the presence of liquid water could be used in studies of convection, precipitation, and severe weather.

5. Conclusions

Line-of-sight integrals of slant water vapor have been made in the Southern Great Plains region of the United States. More than 107 000 measurements spanning 47 days of data in May and June of 2000 were used to compare SW from GPS and a WVR. A linear fit of the GPS SW to the WVR SW produced an rms of 1.3 mm for all observations with a linear correlation coefficient of 0.99. The results presented here illustrate the ability of GPS to measure SW. The GPS technique used here first computed PW, and then determined the nonisotropic component (S_i^j) by computing the unmodeled delay in the direction of each individual satellite.

During certain time periods, there were differences in the GPS and WVR SW even though S_i^j from the two instruments agreed. This implies that there are still systematic differences in the two instruments that need to be resolved before a network of GPS and WVR instruments can be deployed. One possible source of this error may be the mapping functions used to relate low elevation GPS observations to the equivalent zenith value.

Acknowledgments. This research was supported by the Biological and Environmental Research Program (BER), U.S. Department of Energy Grant DE-FG0302ER63327, Dr. Wanda R. Ferrell. We would like to thank Dr. Yoaz Bar- Sever at the Jet Propulsion Lab-

oratory for access to the GPS data used in this study, and two anonymous reviewers for their help.

REFERENCES

Alber, C., R. H. Ware, C. Rocken, and J. J. Braun, 2000: Inverting GPS double differences to obtain single path phase delays. *Geophys. Res. Lett.,* **27,** 2661–2664.

Altamimi, Z., 2001: The International Terrestrial Reference Frame, in International GPS Service for Geodynamics. 1999 IGS Annual Rep. JPL 400-978 07/01, Jet Propulsion Laboratory, 48 pp.

Bar-Sever, Y. E., P. M. Kroger, and J. A. Borjesson, 1998: Estimating horizontal gradients of tropospheric path delay with a single GPS receiver. *J. Geophys. Res.,* **103,** 5019–5035.

Bevis, M., S. Businger, T. A. Herring, C. Rocken, R. A. Anthes, and R. H. Ware, 1992: GPS Meteorology: Remote sensing of atmospheric water vapor using the Global Positioning System. *J. Geophys. Res.,* **97,** 15 787–15 801.

——, ——, S. Chiswell, T. A. Herring, R. A. Anthes, C. Rocken, and R. H. Ware, 1994: GPS meteorology: Mapping zenith wet delays onto precipitable water. *J. Appl. Meteor.,* **33,** 379–386.

Braun, J., C. Rocken, and R. Ware, 2001: Validation of line-of-sight water vapor measurements with GPS. *Radio Sci.,* **36,** 459–472.

Dabberdt, F., and T. W. Schlatter, 1996: Research opportunities from emerging atmospheric observing and modeling capabilities: Report of the Second Prospectus Development Team of the U.S. Weather Research Program. *Bull. Amer. Meteor. Soc.,* **77,** 305–323.

Emanuel, K., and Coauthors, 1995: Report of the First Prospectus Development Team of the U.S. Weather Research Program to NOAA and the NSF. *Bull. Amer. Meteor. Soc.,* **76,** 1194–1208.

Gutman, S. I., and K. Holub, 2000: Ground-based GPS meteorology at FSL. FSL February Forum NOAA, 8 pp.

Hugentobler, U., S. Schaer, and P. Fridez, 2001: Bernese GPS software version 4.2. Astronomy Institute, University of Bern, Bern, Switzerland.

Liljegren, J. C., 2000: Automatic self-calibration of ARM microwave radiometers. *Microwave Radiometer Remote Sensing of Earth's Surface and Atmosphere,* P. Pampalonia and S. Paloscia, Eds., VSP, 433–443.

MacDonald, A. E., Y. Xie, and R. H. Ware, 2002: Diagnosis of three-dimensional water vapor using slant range observations from a GPS network. *Mon. Wea. Rev.,* **130,** 386–397.

Niell, A. E., 1996: Global mapping functions for the atmospheric delay at radio wavelengths. *J. Geophys. Res.,* **101,** 3227–3246.

Rocken, C., R. H. Ware, T. Van Hove, F. Solheim, C. Alber, J. Johnson, M. Bevis, and S. Businger, 1993: Sensing atmospheric water vapor with the Global Positioning System. *Geophys. Res. Lett.,* **20,** 2631–2634.

——, T. Van Hove, and R. H. Ware, 1997: Near real-time GPS sensing of atmospheric water vapor. *Geophys. Res. Lett.,* **24,** 3221–3224.

——, S. Sokolovskiy, J. M. Johnson, and D. Hout, 2001: Improved mapping of tropospheric delays. *J. Atmos. Oceanic Technol.,* **18,** 1205–1213.

Solheim, F. S., R. Vivekanandan, R. H. Ware, and C. Rocken, 1999: Propagation delays induced in GPS signals by dry air, water vapor, hydrometeors and other atmospheric particulates. *J. Geophys. Res.,* **104,** 9663–9670.

Springer, T., 2001: Analysis activities. International GPS Service for Geodynamics, 1999 IGS Annual Rep. JPL 400-978 07/01, Jet Propulsion Laboratory, 48 pp.

Ware, R. H., C. Alber, C. Rocken, and F. Solheim, 1997: Sensing integrated water vapor along GPS ray paths. *Geophys. Res. Lett.,* **24,** 417–420.

Wolfe, D. E., and S. I. Gutman, 2000: Developing an operational, surface-based GPS water vapor observing system for NOAA: Network design and results. *J. Atmos. Oceanic Technol.,* **17,** 426–440.